Journal of Power Sources 185 (2008) 1193–1200

Contents lists available at ScienceDirect

Journal of Power Sources

journal homepage: www.elsevier.com/locate/jpowsour

Predicting Young's modulus of glass/ceramic sealant for solid oxide fuel cell considering the combined effects of aging, micro-voids and self-healing

Wenning Liu*, Xin Sun, Mohammad A. Khaleel

Pacific Northwest National Laboratory, P.O. Box 999, Richland, WA 99354, United States

ARTICLE INFO

Article history:
Received 5 June 2008
Received in revised form 30 June 2008
Accepted 1 July 2008
Available online 17 July 2008

Keywords:
Temperature-dependent modulus
Aging
Micro-damage
Self-healing
Glass/ceramic sealant
SOFC

ABSTRACT

We study the temperature dependent Young's modulus for the glass/ceramic seal material used in solid oxide fuel cells (SOFCs). With longer heat treatment or aging time during operation, further devitrification may reduce the residual glass content in the seal material while boosting the ceramic crystalline content. In the meantime, micro-voids induced by the cooling process from the high operating temperature to room temperature can potentially degrade the mechanical properties of the glass/ceramic sealant. Upon reheating to the SOFC operating temperature, possible self-healing phenomenon may occur in the glass/ceramic sealant which can potentially restore some of its mechanical properties. A phenomenological model is developed to model the temperature dependent Young's modulus of glass/ceramic seal considering the combined effects of aging, micro-voids, and possible self-healing. An aging time-dependent crystalline content model is first developed to describe the increase of the crystalline content due to the continuing devitrification under high operating temperature. A continuum damage mechanics (CDM) model is then adapted to model the effects of both cooling induced micro-voids and reheating induced self-healing. This model is applied to model the glass–ceramic G18, a candidate SOFC seal material previously developed at PNNL. Experimentally determined temperature-dependent Young's modulus is used to validate the model predictions.

1. Introduction

Fuel cells are high-efficiency energy conversion devices that are environmental friendly with little or no toxic emissions. The solid oxide fuel cell continues to show great promise as a future power source, with potential applications in stationary power generation and as auxiliary power units. Among various SOFC designs, anode-supported planar cells have shown great potential in delivering high performance at reasonable costs [1,2]. Planar SOFCs offer a significant advantage of a compact design along with higher power densities. In the meantime, they require the incorporation of hermetic gas seals for efficient and effective channeling of fuel and oxygen.

Seals are the most critical components in commercializing the planar SOFC technology [3–5]. They must adequately prevent the leakage of air and fuel, effectively isolate the fuel from the oxidant, and insulate the cell from short circuit. Essentially, there are two standard methods of sealing: compressive sealing and rigid bonding [6–8]. In compressive sealing, a compliant high-temperature material is captured between the two sealing surfaces and compressed, using a load frame external to the stack, to deliver hermetic sealing. The sealing surfaces can slide with respect to one another without disrupting the hermeticity of the seal. This technology, however, remains incomplete due to the lack of a reliable high-temperature sealing material [9] and the difficulty of designing the appropriate load frame under high operating temperature. Rigid seals rely on effective bonding of the seal material to the sealing surfaces. They offer significant advantages over compressive seals which suffer from problems of oxide scaling and chemical stability under highly reactive environments in addition to the disadvantages of incorporating an externally applied load [6].

As rigid seal, glass joining provides a cost effective and relatively simple method of bonding ceramic and metal parts. However, the softening point of the glass component typically limits the maximum operating temperature to which the joint may be exposed. As discussed by Weil et al. [10], there are a number of other key materials and processing variables that can influence the performance of glass seals, including the composition of the metal substrate against which the seal is made, operating parameters such as the expected lifetime of the device (and therefore the seals), as well as the degree of thermal cycling to which the seals will be exposed during system operation. In addition, glass seal in room temperature is brittle, non-yielding,

* Corresponding author. Tel.: +1 509 372 4967; fax: +1 509 375 2604.
E-mail address: wenning.liu@pnl.gov (W. Liu).

0378-7753/$ – see front matter © 2008 Elsevier B.V. All rights reserved.
doi:10.1016/j.jpowsour.2008.07.017

and particularly susceptible to fracture when exposed to tensile stresses. Because of these, much of the SOFC seal materials development effort has been focused on developing materials that have compatible temperature-dependent CTEs for each of the components being jointed, i.e., the ceramic cell, the seal, and the metal separator, to minimize the build up of residual stresses within the joint. Only a handful of high-temperature glass compositions in the borate- or phosphate-doped aluminosilicate families satisfy these requirements [11]. The glass seal composition used in this study, designated as G18 [12], was developed by PNNL for planar-type SOFC applications. G18 is a barium–calcium–aluminosilicate (BCAS)-based glass with the addition of boron oxide. Silicon-based glasses provide a better combination of chemical compatibility and stability properties than phosphate- or borate-based glasses, although this material is susceptible to chromium migration when used with ferritic stainless steels [13,14]. For rigid bond as such, stress levels in the glass seal and mechanical properties such as Young's modulus and interfacial strength between different interfaces become critical for long-term reliability of the seal and therefore the stacks.

To obtain a reliable SOFC design in the complex operating environments, the stress level in the glass seal materials as well as at the various interfaces must be carefully examined and managed. To accurately predict these stresses, accurate material models considering the various aspects of the seal materials under different operating conditions including aging and cooling become critical.

In this paper, a phenomenological model based on mechanical analogs is developed to describe the temperature-dependent Young's modulus of glass ceramic seal materials. The effects of continuing aging and devitrification on the ceramic phase volume fraction and the resulted mechanical properties of glass ceramic seal material are considered. The effects of micro-voids and self-healing are also considered using a continuum damage mechanics (CDM) model. The formulation is for glass/ceramic seal in general, and it can be further developed to account for effects of various processing parameters. This model was applied to G18, and the temperature-dependent experimental measurements were used to calibrate the modeling parameters and to validate the model prediction.

2. Characteristics of glass–ceramic seal materials

The glass ceramic sealant material examined here, G18, is a barium calcium aluminosilicate-based glass originally melted from the following mixture of oxides (by weight percent): 56.4% BaO, 22.1% SiO_2, 5.4% Al_2O_3, 8.8% CaO, and 7.3% B_2O_3 [12]. The G18 powder was milled to an average particle size of 20 μm and mixed with a proprietary binder system to form a paste that could be dispensed onto the substrate surfaces at a uniform rate of 0.075 g/linear-cm using an automated syringe dispenser. The glass paste may be dispensed onto the YSZ side of the bilayer discs. Each disk was then concentrically positioned on a washer specimen, loaded with a 100 g weight, and heated in air under the following sealing schedule: heat from room temperature to 850 °C at 10 °C min^{-1}, hold at 850 °C for 1 h, cool to 750 °C at 5 °C min^{-1}, hold at 750 °C for 4 h, and cool to room temperature at 5 °C min^{-1} [10].

Silicon-based glasses provide a better combination of chemical compatibility and stability properties than phosphate- or borate-based glasses. The glass wets the surfaces to be bonded at the joining temperature, and subsequent crystallization then provides mechanical stiffness and strength at operating temperatures.

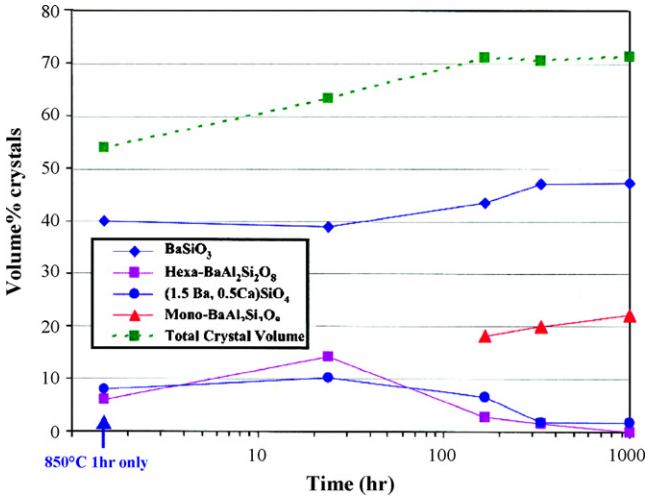

Fig. 1. Quantity of crystalline phase formed in glass ceramic sealant (G18) as a function of time held in air at 750 °C: heating from room temperature to 850 °C at 10 °C min^{-1}, hold at 850 °C for 1 h, cool to 750 °C at 5 °C min^{-1}, hold at 750 °C.

2.1. Aging time-dependent volume fraction evolution of crystalline phase

Aging changes the volume fraction of the ceramic phase in the glass ceramic microstructure, hence influencing seal mechanical properties such as Young's modulus, strength, fracture toughness and durability [15–19]. For glass/ceramic sealing materials, the volume fraction of the ceramic crystalline is aging time-dependent under the SOFC operating temperature. At the end of the initial sealing process at 850 °C, some volume fraction of the ceramic crystalline is formed. Subjected to the typical operating environment of 750 °C, the crystallization process slows down but does not stop. This continuing devitrification causes the volume fraction of the ceramic crystalline in the sealant material to increase with the holding time at the operating temperature. Fig. 1 shows the volume fraction of various crystalline phases formed within the devitrifying G18 as a function of time during 1000 h of aging at 750 °C [10]. This graph was constructed from a series of quantitative X-ray diffraction (XRD) measurements conducted on aged G18 samples.

After 1 h of initial sealing process at 850 °C, the crystalline contents of $BaSiO_3$, $(Ba_{1.5}Ca_{0.5})SiO_4$, and hexa-$BaAi_2Si_2O_8$ are observed in the glass/ceramic seal. $BaSiO_3$ is the main crystalline phase composition, taking up approximately 40% of the volume fraction. After the first 20 h under SOFC working temperature of 750 °C, the volume fractions of both $BaSiO_3$ and $(Ba_{1.5}Ca_{0.5})SiO_4$ remain relatively unchanged, and the volume fraction of hexa-$BaAi_2Si_2O_8$ doubled from 7 to 15%. With longer working time, the content of $(Ba_{1.5}Ca_{0.5})SiO_4$ and the hexa-$BaAi_2Si_2O_8$ began to decrease, and the content of $BaSiO_3$ started to increase. A new phase of mono-$BaAi_2Si_2O_8$ starts to appear at about 150 h of working time and continues to increase because $(Ba_{1.5}Ca_{0.5})SiO_4$ and hexa-$BaAi_2Si_2O_8$ are both transformed into this phase. The overall crystalline phase increases almost linearly with log (time(h)) in the first 300 h of aging. After that, the crystallization process gradually stops and the crystalline content in the material remains relatively unchanged.

Assuming the devitrification of glass/ceramic can reach an asymptotic level after 300 h of aging/working time at 750 °C, the evolution of the volume fraction of the crystalline phases with respect of time t may be expressed as

$$f_C(t) = f_C^{\infty} - (f_C^{\infty} - f_C^0)e^{(-t/A_t)} \quad (1)$$

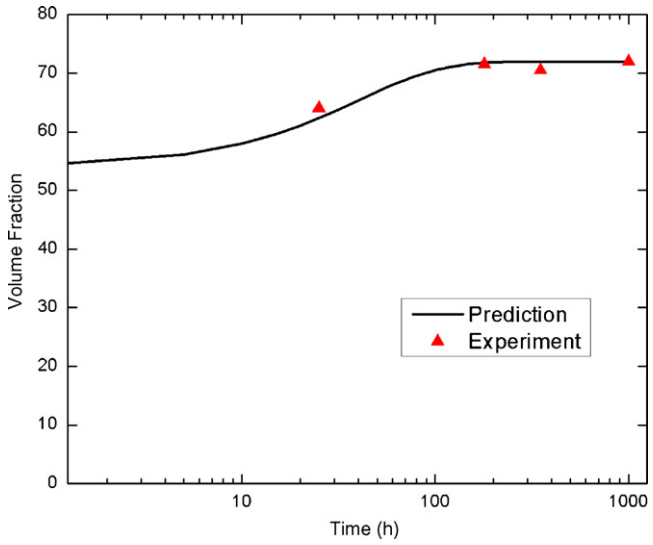

Fig. 2. Comparison of Eq. (1) and experimentally measured crystalline phase volume fraction for G18.

where f_C^∞ and f_C^0 represent the volume fractions of the ceramic phase in the stable stage and the initial stage of the sealing process, respectively. A_t represents the characteristic aging time. Note that various crystalline phases are lumped into one term, f_C, in this work.

According to the experimental data shown in Fig. 1, the parameters in Eq. (1) can be determined for G18 as

$$f_C^\infty = 72.0, \quad f_C^0 = 54.0, \quad A_t = 40.0(\text{h}) \tag{2}$$

These are material-specific parameters that are closely dependent on the glass composition and associated heat treatment processes. Fig. 2 compares the crystalline volume fraction evolution expressed by Eq. (1) with the experimental measurements shown in Fig. 1. Clearly, the overall evolution trend of the crystalline phase can be captured well by Eq. (1).

2.2. Aging-induced micro-voids in glass–ceramic

Aging at high temperature often leads to material property degradations [20,21]. One possible degradation mechanism is the appearance of the voids and cracks [22]. For example, Fig. 3 shows the microstructure of the glass ceramic sealant after the glass paste is sintered. At the end of the initial sealing process, distinct boundaries between the glass (amorphous) phase and ceramic (crystalline) phase can be observed, and the fibrous and needle-like crystalline structures can be seen clearly in the amorphous glass phase. Some small voids and flaws are also illustrated in the microstructures.

As further devitrification takes place and the volume fraction of the crystalline phases increases, morphology of the crystalline phases also changes, leading to less fibrous needles and more diffused phase boundaries. Fig. 4 shows the room temperature microstructure of G18 after aging at 750 °C for 1000 h. Many more small voids are now present, particularly in the amorphous phase, and the overall void volume fraction is also increased from Fig. 3. The micro-voids are possibly caused by the CTE difference between the ceramic and the glass phase during cooling. Different shrinkages of the two phases will likely induce some voids in the glass phase which has lower thermal expansion coefficients compared to the ceramic phase [23–25]. Compared with Fig. 3, the distinct fibrous and needle-like crystalline in the amorphous phase disappeared, and smeared/diffused phase boundaries between the glass phase and ceramic phase are observed after 1000 h aging.

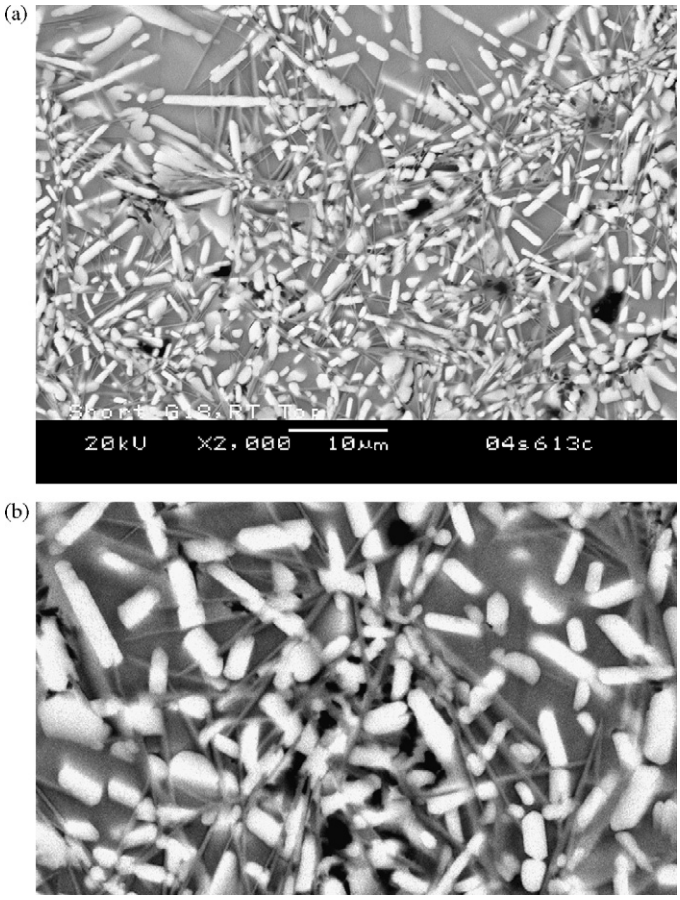

Fig. 3. SEM image of microstructure of G18 after sintering process—heat from room temperature to 850 °C at 10 °C min^{-1}, hold at 850 °C for 1 h, cool to 750 °C at 5 °C min^{-1}, hold at 750 °C for 4 h, and cool to room temperature at 5 °C min^{-1}: (a) magnification: 2000× and (b) magnification: 5000×.

To capture the effect of aging and cooling induced microstructure changes on the mechanical property of the glass ceramic sealant, a continuum damage mechanics model [26–29] is used here as a phenomenological approach to the constitutive modeling of glass/ceramic seal. The microstructure-level heterogeneous G18 is represented by an equivalent homogeneous material with effective properties. The model accounts for the material damage because of various mechanisms (i.e., void growth, void nucleation and coalescence, decohesion between different phases, etc.) in a phenomenological way through a scalar damage variable, D, that governs the reduction of the homogenized elastic modulus [29]:

$$E^{\text{D}}(t, T, D) = E(t, T)(1 - D) \tag{3}$$

where E^{D} and E represent the Young's modulus with and without damage, t is time and T is temperature. D is the quantitative measure of the void volume fraction in comparison with the virgin microstructure.

2.3. Possible self-healing of glass–ceramic seals

Even though G18 exhibits creep/flow behavior under operating temperature, its behavior at room temperature can be characterized as being brittle. During thermal cycling, the tensile residual stresses caused by the mismatch of CTE of various cell components can potentially generate many small cracks and voids in the brittle seal material after cool down. If left untreated/unhealed, these

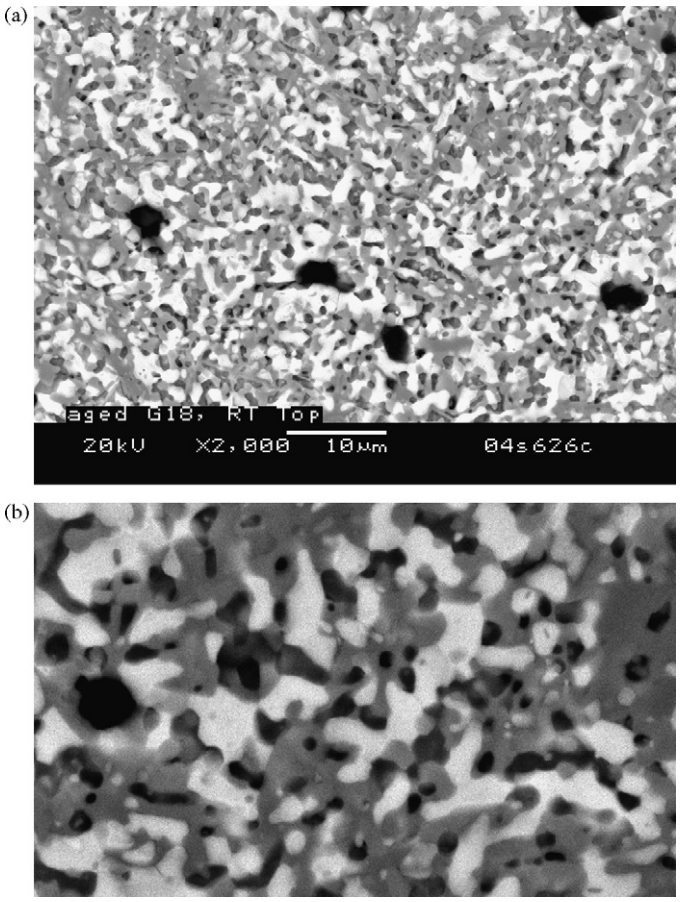

Fig. 4. SEM image of microstructure of G18 after 1000 h aging: (a) magnification: 2000× and (b) magnification: 5000×.

small cracks in the seal could be detrimental to the overall stack reliability for the next operating cycle.

In order to examine the seal microstructures upon reheating, room temperature Vickers indentation tests and subsequent reheating is performed on G18. Fig. 5 shows a typical room temperature Vickers indentation impression on the surface of the short crystallized G18. With a 2 kg indentation load, four perfectly symmetrical radial cracks are generated emanating from four corners

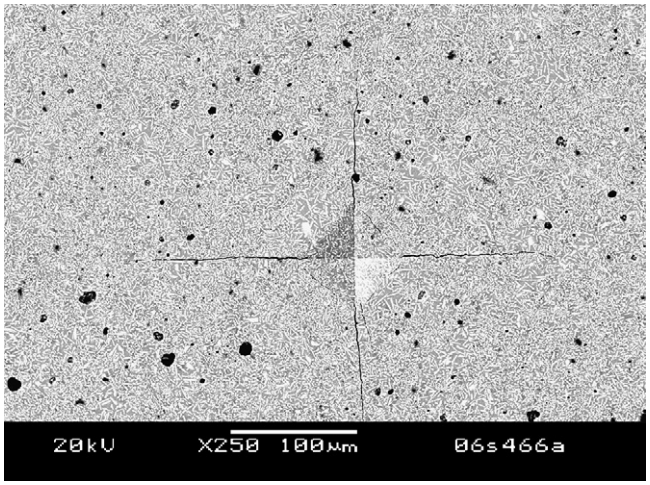

Fig. 5. Typical Vickers impression at 2 kg indentation load at room temperature on polished G18 short crystallized.

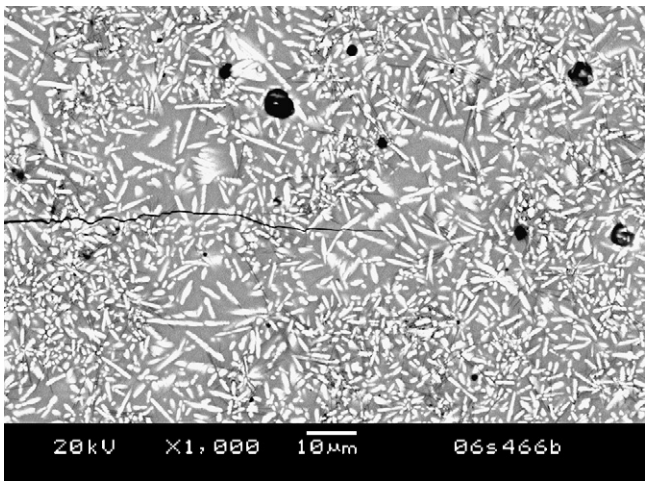

Fig. 6. SEM pictures at the crack tip on polished G18 short crystallized with higher magnification.

of the indentor edge. Under higher magnification in Fig. 6 for one of the radial cracks, it is observed that crack propagation followed a less tortuous path as compared to typical structural ceramics [30,31]. The white crystallite in rod shape (likely $BaSiO_3$) appears to be stronger than the featureless glass (gray area) since some crack deflection and bridging was observed as compared to the straight crack path through the gray area (likely the un-crystallized residual glasses). Nevertheless, the G18 showed typical brittleness with single crack at room temperature.

After indentation, the sample was held at 750 °C for half an hour. Figs. 7 and 8 show the typical SEM image of the original indentation impression of the example at low and high magnifications, respectively. It may be seen that all the four radial cracks completely disappeared, even under higher magnification. These experimental observations can serve as evidence that the glass/ceramic sealant material G18 does exhibit some degree of self-healing: when reheated again to high operating temperature, the damage in the glass ceramic sealant may disappear due to the flow of the glass phase, potentially restoring its mechanical property to its undamaged level. Other possible physical explanations for this healing behavior may be the capillary force of the residual glass phase as well as the residual stresses caused by the Vickers indentation.

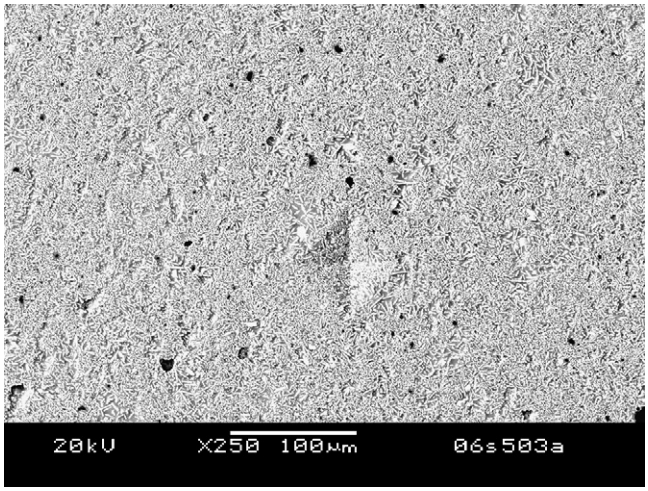

Fig. 7. SEM pictures at the impression on polished G18 short crystallized: after indentation, the sample was held at 750 °C for half an hour.

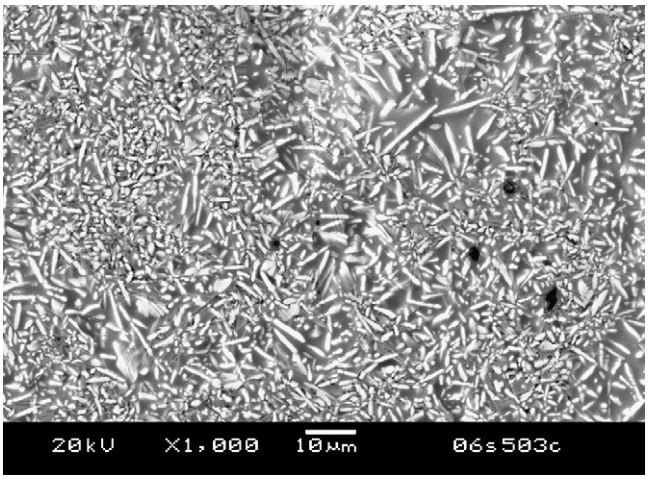

Fig. 8. SEM pictures at the impression tip on polished G18 short crystallized: after indentation, the sample was held at 750 °C for half an hour.

It should be mentioned that the concept of self-healing glass seals was first reported by Singh [32]. The rationale behind this concept is that at the SOFC operating temperature, a sealing glass with appropriate properties can heal cracks created during thermal transients. The advantage of this approach is that materials with dramatically different expansion can potentially be used for seals, because at the cell operating temperatures, CTE mismatch-induced thermo-mechanical stresses can be relaxed out. If proven feasible, this type of seals can tolerate some of the thermal expansion mismatch and still form a functioning seal between materials with significant expansion mismatch. However, there are still a number of challenges in making a functioning seal with self-healing glasses. The first challenge is that the glass seal must maintain contact with all the components to be sealed without excess creep/flow at cell operating temperature of 750 °C. Concepts involving various ceramic phase stoppers have been proposed to address this. In addition, the self-healing glass seal must be able to remain chemically stable under SOFC operating temperature for the designed stack operating time.

For SOFC stacks under deep thermal cycles, cracking and micro-voids may occur in the glass ceramic sealant due to the tensile residual stress caused by CTE mismatch of different components during cooling. However, upon reheating, the damage/crack may be healed at temperatures above some threshold temperature due to the flow behavior of the glass phase. Therefore, the scalar damage D defined in Eq. (3) is temperature and aging time-dependent, which may be simplified as the product of the following uncoupled factors:

$$D = A_D D_T \tag{4}$$

Here A_D is the aging influence function, representing the increase of micro-void volume fraction with aging time:

$$A_D = 1 - e^{-t/t_c} \tag{5}$$

where t is the aging time, and t_c represents the characteristic time.

D_T in Eq. (4) represents the temperature-dependence of damage, reflecting the possible self-healing behavior of G18 above the threshold temperature, T_{th}:

$$D(T) = D_0 \frac{\pi/2.0 - \arctan[(T - T_{th})/R]}{\pi} \tag{6}$$

where D_0 is damage parameter at room temperature, and T_{th} is the threshold temperature above which damage of the glass ceramic composite starts to heal, and R is a constant.

3. Assembly of the phenomenological model

Various formulation and framework have been developed to model the mechanical behavior of composite materials [33–38]. For simplicity, we adopt here the simple Rule of Mixture approach. In general, the Young's modulus of the multi-phase composite materials can be expressed as [39]:

$$E = \sum_{i=1}^{m} f_i E_i \tag{7}$$

where f_i and E_i represent the volume fraction and modulus of the ith phase, and m is the number of the phases in the composite material. The volume fractions of all the phases should satisfy:

$$\sum_{i=1}^{m} f_i = 1 \tag{8}$$

In the case of the two-phase glass/ceramic sealant composite material, the above equation can be rewritten as

$$E = f_C E_C + (1 - f_C) E_G \tag{9}$$

or

$$E = f_C (E_C - E_G) + E_G \tag{10}$$

where subscripts "C" and "G" refer to glass phase and ceramic phase, respectively. In general, the modulus of the glass phase is temperature dependent, and modulus of the ceramic crystalline is independent of temperature.

Substituting the aging time dependent volume fraction of the ceramic phase, i.e., Eq. (1), into Eq. (10) leads to:

$$E(t, T) = (f_C^{\infty} - f_C^0 e^{(-t/A_t)})(E_C - E_G(T)) + E_G(T) \tag{11}$$

Incorporating the effects of micro-damage and self-healing described in Eqs. (3)–(6) into Eq. (11) yields the following phenomenological model describing the elastic modulus of the glass ceramic materials:

$$E^D(t, T, D) = [(f_C^{\infty} - f_C^0 e^{(-t/A_t)})(E_C - E_G(T)) + E_G(T)] \times \left\{1 - \frac{D_0}{\pi}(1 - e^{-t/t_c}) \left[\frac{\pi}{2.0 - \arctan\left(\frac{T - T_{th}}{R}\right)}\right]\right\} \tag{12}$$

Again f_C^{∞} and f_C^0 represent the volume fractions of the ceramic phase in the stable stage and at the initial stage of the sealing process, respectively. A_t represents the characteristic aging time. D_0 is the damage parameter at room temperature, and T_{th} refers to the threshold temperature above which damage of the glass ceramic composite starts to heal. R is a material constant, t is the aging time, and t_c represents the characteristic time for aging induced micro-damage.

4. Comparison between experimental measurements and predictions

4.1. Temperature-dependent modulus measurements

The dynamic resonance technique (ASTM C1198) was used to measure the elastic moduli of the specimens of both non-aged and 1000 h aged short crystallized G18 at room and elevated temperatures [40]. The instrument used to measure the resonant frequencies was constructed following ASTM C1198. The specimen was suspended within a resistance-heated furnace using single-crystal sapphire fibers with beaded ends. Small, narrow notches were cut into the corners of the specimen to accept the fibers.

Table 1
Young's modulus aged and un-aged G18 at room and elevated temperatures

Temperature (°C)	1000 h Aged (GPa)	Un-aged (GPa)
22	60.8 ± 0.3	77.7 ± 0.4
200	61.0 ± 0.3	75.8 ± 0.4
300	62.2 ± 0.3	74.3 ± 0.4
400	69.7 ± 0.3	71.7 ± 0.3
500	70.2 ± 0.3	70.6 ± 0.3
600	70.3 ± 0.3	67.7 ± 0.3
700	69.2 ± 0.3	–
800	67.4 ± 0.3	–
30	53.2 ± 0.3	78.1 ± 0.4

The fibers coupled the specimen to two piezoelectric transducers mounted above the furnace. One transducer was used as a driver, and the other as a receiver. A computer-controlled system was used to send frequency signals sweeping from 20 Hz to 20 kHz through the driver transducer. The signal from the receiving transducer was fed back into the computer, and the resonant frequencies were identified and recorded. Both the transverse and longitudinal resonant frequencies could be reliably detected at the corners of the specimen. Resonant frequency data were then used in calculating the elastic moduli with the following equations [41]:

$$E = 0.9465\frac{mf_f^2}{b}\frac{L^3}{h^3}T_1 \quad (13)$$

$$G = \frac{4Lmf_t}{bh}\frac{B}{1+A} \quad (14)$$

where E and G are the Young's modulus and shear modulus, respectively; m is the mass of the bar, b, h and L are the width, thickness, and length of the bar, respectively. f_f represents the fundamental resonant frequency of the bar in flexure; and T_1 denotes the correction factor for fundamental flexural mode to account for the finite thickness of the bar and Poisson's ratio, etc. The Young's and shear moduli were then used to calculate Poisson's ratio:

$$\mu = \left(\frac{E}{2G}\right) - 1 \quad (15)$$

The precisions of the E, G and μ values were calculated by propagating the uncertainty of each term through the equations.

The test specimen was a right parallelepiped measuring 50.75 mm × 25.34 mm × 5.96 mm. All surfaces were ground smooth. Resonant frequencies were measured at room temperature and in 100 °C intervals from 200 to 800 °C. The furnace was heated at a rate of approximately 12 °C min^{-1}, and was held for 15 min at each temperature for equilibration.

The measured Young's modulus for the non-aged and 1000 h aged G18 at room and elevated temperature is tabulated in Table 1. Both of the measured Young's modulus and shear modulus for the non-aged and 1000 h aged G18 at room and elevated temperature are shown in Fig. 9. For non-aged short crystallized glass/ceramic sealant (G18), both the Young's modulus and shear modulus decrease with increasing test temperature. The resonant peaks became very broad at about 700 °C, making it impossible to differentiate between the longitudinal and transverse peaks with any certainty. This may have been caused by the softening of the glass phase present in these specimens. Additional measurements taken again at room temperature (30 °C) after the high-temperature tests achieve the same moduli as the pre-test values.

The measured Young's modulus and shear modulus for the 1000 h aged G18 show some very distinct and interesting features. For temperatures lower than 400 °C, both Young's modulus and shear modulus increase with increasing test temperature. The moduli exhibit somewhat temperature independent behaviors from

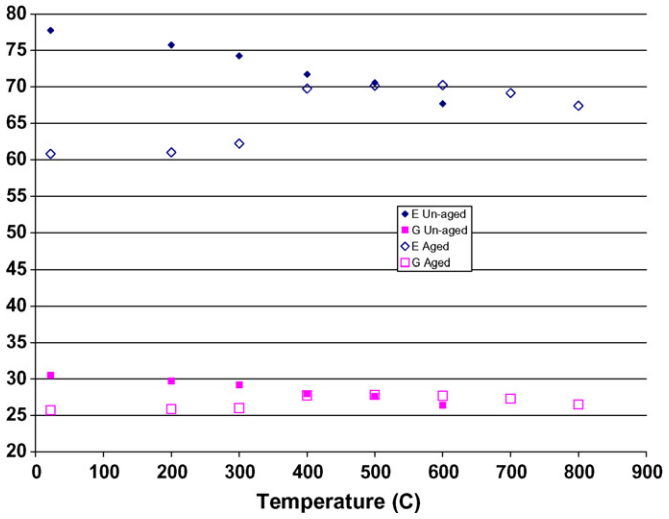

Fig. 9. Young's and shear moduli for aged and un-aged G18 at room and elevated temperature: the furnace was heated at a rate of approximately 12 °C min^{-1}, and was held for 15 min at each temperature for equilibration.

400 to 600 °C. Above 600 °C, the moduli start to decrease with increasing temperature.

For temperatures lower than 400 °C, the measured modulus for the aged glass ceramic sealant is consistently less than that of the non-aged (short-term aged) glass ceramic. At about 500 °C, the moduli for the aged and non-aged samples cross over. For temperatures above 600 °C, the moduli trend reverses itself: the modulus for 1000 h aged G18 is higher than that of the non-aged G18.

This distinct temperature-dependent modulus behavior for the aged G18 is another motivation for our current work. Our goal is to see whether this unique behavior can be predicted by coupling the various phenomena such as aging, cooling and reheating induced self-healing. The eventual goal is to develop the predictive capability for glass ceramic seals such that better seal materials can be developed for improved reliability and durability.

4.2. Modeling results

For the phenomenological model described in Eq. (12), the modulus of the ceramic phase is considered to be temperature independent, and modulus for the glass phase is considered to be temperature dependent. In general, the Young's modulus of glass drops dramatically over the glass transition temperature, T_g [42].

The input Young's moduli used for the glass and crystalline phases are shown in Fig. 10 in dashed lines [42]. The predicted Young's moduli of G18 under different aging times are shown in solid lines in Fig. 10. The following parameters for Eq. (12) are calibrated based on the experimental data:

$$D_0 = 0.24, \quad T_{th} = 375\,^\circ\text{C}, \quad R = 50\,^\circ\text{C}, \quad t_c = 100\,\text{h}$$

With the proposed phenomenological model, reasonably good comparisons between the predicted and measured Young's modulus have been achieved for both the aged and un-aged G18. This is particularly true for temperatures lower than 600 °C. Above 600 °C, the predicted modulus decreases more rapidly with temperature than the measured data. This is because the predicted modulus is very sensitive to the input temperature-dependent modulus for the glass phase. For temperatures above 600 °C, the Young's modulus for glass may vary dramatically [43,44]. The exact high-temperature Young's modulus for regular glass is rarely reported, and the high-temperature Young's modulus for the glass phase in G18 has not yet been separately determined. Therefore for temper-

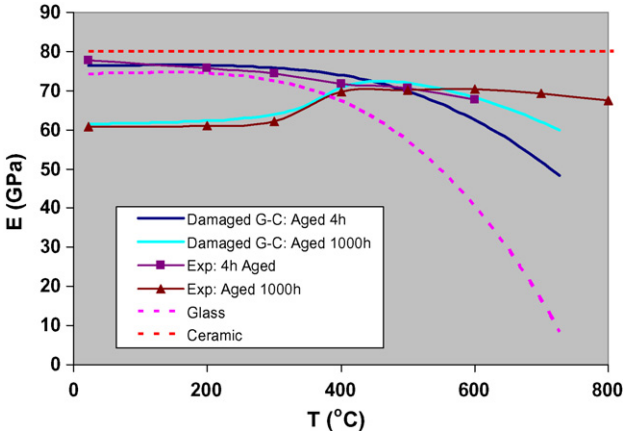

Fig. 10. Predicted and measured Young's modulus vs. temperature.

atures above 600 °C, the glass moduli used in Fig. 10 could have been much lower than the actual values.

It is interesting to note that, by considering the combined effects of aging, micro-voids and self-healing, the distinct feature of the moduli 'cross-over' can be predicted by the simple phenomenological model: Below 500 °C, the 1000 h aged sample has lower Young's modulus compared to the 4 h aged sample; Above 500 °C, the trend reverses itself when considering self-healing of the glassy phase.

5. Conclusions

We study the temperature-dependent Young's modulus of G18, a glass ceramic material for SOFC sealing applications. The combined effects of aging, cooling-induced micro-voids and possible reheating related self-healing are examined and modeled with some simple, phenomenological models. After the initial sealing process, the crystallization process of G18 slows down but does not stop, and the volume fraction of the crystalline phase increases with aging/working time. In addition, aging causes the diffusion/smearing of the boundaries between the crystalline and the amorphous phases and potentially changes the mechanical properties of the amorphous phase.

Upon cooling to room temperature, shrinkage micro-voids will be formed because of the CTE differences between the crystalline and the amorphous phases. On the stack level, cooling induced micro-cracks are also likely to occur due to the CTE mismatch between different stack components. These micro-voids and micro-cracks can noticeably degrade the Young's modulus of the glass ceramic seal at room temperature. However, when reheated back to SOFC working temperature, this study shows that G18 does exhibit some degree of self-healing behaviors because of the flow characteristics of the glass phase at high temperatures. Therefore the mechanical property, i.e., Young's modulus of the glass/ceramic seal material can be potentially restored to its undamaged level at high temperatures.

The phenomenological model based on some simple mechanical analogs is developed to capture the above-described mechanical behaviors of glass ceramic seal materials. The aging time dependent crystalline phase evolution model was first developed to describe the increase of crystalline content due to the continuing devitrification during operation. A continuum damage mechanics model was adapted to model the effects of micro-voids and self-healing. Reasonably good comparisons between the measured and the predicted temperature-dependent Young's modulus have been obtained. The modeling parameters presented here are calibrated with the experimental data for G18, yet the modeling framework should be applicable to glass/ceramic seal in general. The model can be further developed to account for the effects of various processing parameters on the mechanical properties of glass/ceramic seal materials.

Acknowledgements

The Pacific Northwest National Laboratory is operated by Battelle Memorial Institute for the United States Department of Energy under Contract DE-AC06-76RL01830. The work was funded as part of the Solid-State Energy Conversion Alliance (SECA) Core Technology Program by the U.S. Department of Energy's National Energy Technology Laboratory (NETL).

References

[1] W.P. Teagan, J.H.J.S. Thijssen, E.J. Carlson, C.J. S Read, in: A.J. McEvoy (Ed.), Proceedings of the 4th European Solid Oxide Fuel Cell Forum, vol. 2, Lucerne, Switzerland, 2000, pp. 969–980.
[2] B.W. Chung, C.N. Chervin, J.J. Haslam, A. Pham, R.S. Glass, Journal of the Electrochemical Society 152 (2) (2005) A265–A269.
[3] K.A. Nielsen, M. Solvang, S.B.L. Nielsen, A.R. Dinesen, D. Beeaff, P.H. Larsen, Journal of the European Ceramic Society 27 (2/3) (2007) 1817–1822.
[4] S.R. Choi, N.P. Bansal, Mechanical, Ceramic Engineering and Science Proceedings 26 (4) (2005) 275–283.
[5] F. Smeacetto, M. Salvo, M. Ferraris, J. Cho, A.R. Boccaccini, Journal of the European Ceramic Society 28 (1) (2008) 61–68.
[6] R.N. Singh, International Journal of Applied Ceramic Technology 4 (2) (2007) 134–144.
[7] J.W. Fergus, Journal of Power Sources 147 (2005) 46–47.
[8] Y.S. Chou, J.W. Stevenson, L.A. Chick, Journal of America Ceramic Society 86 (6) (2003) 1003–1007.
[9] S.P. Simner, J.W. Stevenson, Journal of Power Sources 102 (2001) 310–316.
[10] K.S. Weil, J.E. Deibler, J.S. Hardy, D.S. Kim, G.G. Xia, L.A. Chick, C.A. Coyle, Journal of Materials Engineering and Performance 13 (3) (2004) 316–326.
[11] N. Lahl, L. Singheiser, K. Hilpert, K. Singh, D. Bahadur, Proceedings of the 6th International Symposium on Solid Oxide Fuel Cells, Pennington, NJ, 1999, pp. 1057–1065.
[12] K.D. Meinhardt, J.D. Vienna, T.R. Armstrong, L.R. Pederson, U.S. Patent 6,430,966, 2002.
[13] Z. Yang, K.D. Meinhardt, J.F. Stevenson, Journal of the Electrochemical Society 150 (8) (2003) A1095–A1101.
[14] Z. Yang, G. Xia, K.D. Meinhardt, K.S. Weil, J.W. Stevenson, Journal of Materials Engineering and Performance 13 (3) (2004) 327–334.
[15] W.T. Han, M. Tomozawa, Journal of American Ceramic Society 72 (10) (1989) 1837–1843.
[16] N. Bhathena, R.G. Hoagland, G. Meyrick, Journal of the American Ceramic Society 67 (12) (1984) 799–805.
[17] A. Bentur, M. Ben-Bassat, D. Schneider, Journal of the American Ceramic Society 68 (4) (1985) 203–208.
[18] I. Schwarz, M. Stranz, M. Bonnet, J. Petermann, Collid Polymer Science 279 (2001) 506–512.
[19] C. Baudin, M.P. Villar, Journal of the American Ceramic Society 81 (10) (1998) 2741–2745.
[20] J. Nam, J.C. Seferis, Journal of Polymer Science, Part B: Polymer Physics 30 (1992) 455–463.
[21] J. Nam, J.C. Seferis, Journal of Polymer Science, Part B: Polymer Physics 29 (1991) 601–608.
[22] J. Kim, W. Lee, S.W. Tsai, Composites: Part B 33 (2002) 531–543.
[23] C. Roos, O. Becker, F. Siebers, Journal of Materials Science 42 (2007) 50–58.
[24] M. Brochu, B.D. Gauntt, R. Shah, G. Miyake, R.E. Loehman, Journal of the European Ceramic Society 26 (15) (2006) 3307–3313.
[25] Y. Fei, Mineral Physics and Crystallography, A Handbook of Physical Constants, AGU Reference Shelf 2, The American Geophysical Union, 1995.
[26] S.M. Jessen, A. Plumtree, Composites 22 (3) (1991) 181–190.
[27] J. Jeong, H. Adib, G. Pluvinage, Journal of Non-Crystalline Solids 351 (24–26) (2005) 2065–2075.
[28] J. Lemaitre, in: O. Allix, F. Hild (Eds.), Continuum Damage Mechanics of Materials and Structures, Elsevier Science Ltd., Amsterdam, 2002, pp. 235–258.
[29] X. Sun, W.N. Liu, W. N. Chen, D. Templeton, Journal of Impact Engineering, in press.
[30] Y. Fang, K. Ravi-Chandar, K.W. White, Journal of the American Ceramic Society 85 (7) (2002) 1783–1787.
[31] C. Marliere, F. Despetis, J. Phalippou, Journal of Non-Crystalline Solids 316 (1) (2003) 21–27.
[32] R.N. Singh, Journal of Materials Engineering and Performance 15 (4) (2006) 422–426.
[33] D. Bigaud, P. Hamelin, Composite Structures 38 (1–4) (1997) 361–371.
[34] S.R. Annapragada, D. Sun, S.V. Garimella, Computational Materials Science 40 (2) (2007) 255–266.

[35] I.W. Chen, A.S. Argon, Acta Metallurgica 27 (1979) 785–791.
[36] P. Leble, M. Dong, S. Schmauder, Computational Materials Science 15 (1999) 455–465.
[37] S. Ahzi, A. Makradi, R. Gregory, D. Edie, Mechanics of Materials 35 (2003) 1139–1148.
[38] A. Makradi, S. Ahzi, R.V. Gregory, D.D. Edie, International Journal of Plasticity 21 (4) (2005) 741–758.
[39] R.F. Gibson, Principles of Composite Material Mechanics, CRC Press, 2007, pp. 91–101.
[40] D.L. Shelleman, D.J. Green, Measurement of Elastic Constants on Sample Supplied by PNNL, Internal Technical Report, 2006.
[41] Standard Test Method for Dynamic Young's Modulus, Shear Modulus, and Poisson's Ratio for Advanced Ceramics by Sonic Resonance, ASTM, 2008, p. C1198.
[42] D.A. McGRAW, Journal of the American Ceramic Society 35 (1) (1952) 22–27.
[43] E.L. Bourhis, P. Gadaud, J.P. Guin, N. Tournerie, X.H. Zhang, J. Lucas, T. Rouxel, Scripta Materilia 45 (2001) 317–323.
[44] J.P. Andrews, Proceedings of the Physical Society 36 (1924) 169–177.